Journal of Petroleum Science and Engineering 210 (2022) 109834

Contents lists available at ScienceDirect

Journal of Petroleum Science and Engineering

journal homepage: www.elsevier.com/locate/petrol

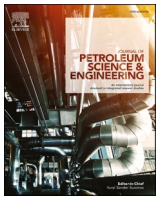

Meteoric freshwater leaching and its significance to reservoir quality in a buried hill of lower-middle Jurassic fluvial sandstones: A case study from the Huanghua Depression, Bohai Bay Basin, China

Zhukun Wang [a,b,c,*], Yingchang Cao [a,b,**], Rudy Swennen [c], Guanghui Yuan [a,b], Ke Wang [a,b]

[a] School of Geosciences, China University of Petroleum, Qingdao, 266580, China
[b] Laboratory for Marine Mineral Resources, Qingdao National Laboratory for Marine Science and Technology, Qingdao, 266071, China
[c] Department of Earth and Environmental Sciences, KU Leuven, Celestijnenlaan 200E, 3001, Leuven, Belgium

ARTICLE INFO

Keywords:
Secondary porosity
Meteoric freshwater
Buried hill
Jurassic
Huanghua depression
Bohai Bay Basin

ABSTRACT

Within polycyclic sedimentary basins, meteoric freshwater leaching plays an important role in the formation of secondary porosity. Whereas, when superimposed by other late diagenesis processes, it is often difficult to identify its diagenetic indicators. The Jurassic clastic reservoirs in the "Wmy buried hill" of the Huanghua Depression testify from such meteoric freshwater diagenesis. The "buried hill" is named after a village called "Wmy" and nowadays buried deeply into a Paleogene lacustrine sag, which displays like a highland or hill. These reservoir sandstones were studied based on a variety of approaches including 3-D seismic interpretation, core and thin section observations, X-ray fluorescence analysis, Electron Probe Microanalysis and stable isotope analysis, combined with reconstruction of the burial and thermal histories. At last, the evolutionary model of reservoir quality was addressed. Difference of sedimentary fabrics in sand bodies leads to the heterogeneity of pores distribution, making the permeability in coarse-grained and fine-grained sandstones largely different. The meteoric water leaching caused the loss of Fe and Ti, leading to a zonation of core colors with white and red zones. In addition, the dissolution by meteoric water of biotite and volcanic fragments as well as feldspar grains produced large amounts of secondary porosity without formation of diagenetic by-products, which thus points to an open diagenetic system. The calcite cement of meteoric freshwater origin displays relatively low Fe and high Mn content exhibiting a low Fe/Mn ratio. The origin of Mn is probably dissolution of volcanic fragments. The evolutionary process of reservoir quality can be divided into four stages. The second stage is the crucial period for formation of secondary porosity whilst faults derived from the compressional stress during tectonic uplif associate coal-bearing source rocks with Jurassic reservoirs. Moreover, the last stage is the critical period for petroleum and/or gas migration and accumulation because the underlying coal-measures entered the hydrocarbon generation window and overlying Paleogene sealing rocks were intensely compacted. Scale of potential reservoirs in the whole well profile are evaluated by statistical methods, the total thickness of which can reach about 25 m. Reservoirs close to the unconformity surface between the Mesozoic and Cenozoic display more effective porosity than the deeper ones, which should be the target for the subsequent hydrocarbon exploration.

1. Introduction

As the definition points out, "buried hills" are ancient highs which are covered by younger formations, meaning there must exist an unconformity between the two suites of strata that possess distinct geological ages (Powers, 1922, 1926). From then onwards hydrocarbons derived from "buried hills" have been attracting much attention from geologists, particularly petroleum geologists all over the world (Tomlinson, 1926; Walters, 1946; Landes et al., 1960; P'An, 1982; Qi and Xie-Pei, 1984; Tong and Huang, 1991; Meng et al., 2009; Zhao et al., 2015). In these papers, almost all the "buried hills" consist of crystalline rocks with reservoir space corresponding mainly to fractures, fissures and cavities, most of which correspond to igneous and metamorphic basements. In contrast sedimentary rocks that originate from

* Corresponding author. School of Geosciences, China University of Petroleum, Qingdao, 266580. China.
** Corresponding author. School of Geosciences, China University of Petroleum, Qingdao, 266580, China.
E-mail address: wangzhukun1126@163.com (Z. Wang).

https://doi.org/10.1016/j.petrol.2021.109834
Received 5 June 2021; Received in revised form 5 October 2021; Accepted 11 November 2021
Available online 13 November 2021

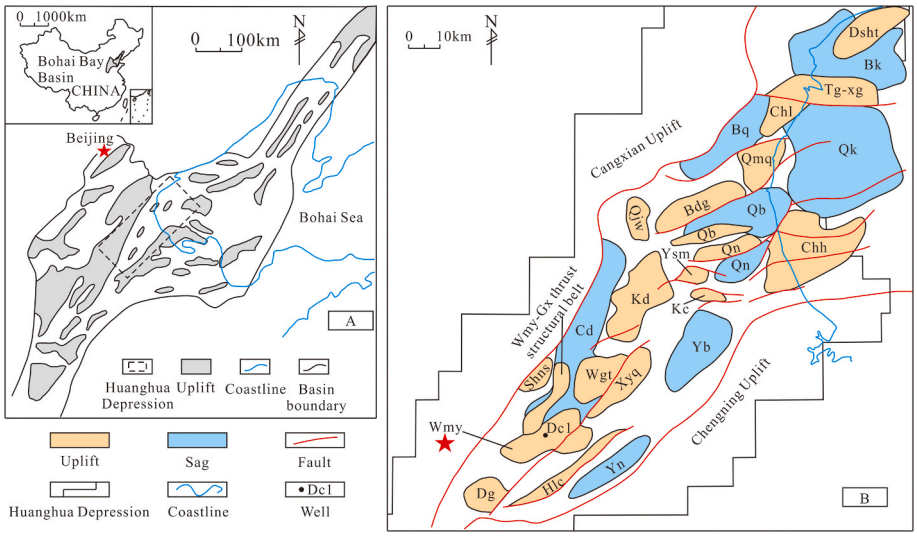

Fig. 1. (A) Location of the Huanghua Depression in Bohai Bay Basin, NE China; (B) Location of the "Wmy buried hill" in the Huanghua Depression showing the distribution of all "buried hills" (modified from Zhao et al., 2019). The blank area in Figure B represents tectonic slopes.

mechanical transport and sedimentation (Sam Boggs, 2006) may hold much primary porosity even when they were deeply buried. Although faults, fractures and veins can still form in sedimentary rocks like crystalline units, remnant primary porosity is particularly helpful to transfer acid diagenetic fluids to form secondary porosity (Schmidt and Mcdonald, 1979a, b). During epidiagenesis, meteoric freshwater carrying carbon dioxide can form carbonic acid solutions, thus leaching of unstable clastic phases can give rise to secondary porosity (Bjørlykke et al., 1992; Emery et al., 1990; Hrabar and Potter, 1969; Ramm, 1992; Schmidt and Mcdonald, 1979a). In this respect the lower limit that meteoric water can infiltrate below an unconformity and along faults is of importance and reported depths can exceed 2 km (Purvis, 1995; Yuan et al., 2015a, 2017).

Located in the southernmost part of the Huanghua Depression in the Bohai Bay Basin of China, the so-called Wmy clastics occur in a typical "buried hill" setting, which was deposited in the lower to middle Jurassic and latter was intensely eroded in the late middle Jurassic to the early Paleogene. The reservoir sandstones underwent a relatively simple burial history followed by tectonic uplift before being buried again. It thus serves as an ideal example for studying the correlation between meteoric freshwater leaching and potential enhanced secondary porosity development in a "buried hill" setting within clastic rocks. Furthermore, two types of colored zones respectively red and white are observed in the cores, which are parallel to strata at a certain angle with respect to the unconformity surface. Hence, with the zonation occurring, selective diagenetic features and the comprehension of its effect on the development of secondary porosity, which is tightly associated with hydrocarbon exploration, is addressed.

2. Geological setting

The Huanghua Depression, as a sub-tectonic unit, is located in the middle part of the Bobai Bay Basin (NE-China) (Fig. 1A). This depression has a southwest to northeast orientation (37°30 ' -39°50 ' N and 116°10 ' -119°30 ' E) and covers an area of approximate 18,500 km^2. It is delineated by the Yanshan fold belt in the north, the Cangxian Uplift in the west and the Chengning Uplift in the east (Zhang et al., 2008; Zhao et al., 2018). In the depression, more than 10 "buried hills" composed of carbonate, clastic or igneous rocks were found since the 1960s (Fig. 1B). The Huanghua Depression formed on the basis of a pre-Jurassic craton and was later covered by Mesozoic and Cenozoic cover layers. The tectonic evolution can be subdivided into three stages, i.e. regional compression (Triassic-early Cretaceous), tectonic subsidence (Paleogene) and regional subsidence (Neogene-Quaternary). In the first stage, a separation in the Indosinian, early and late Yanshan movements can be differentiated. As a consequence, the Mesozoic formation in the depression includes the lower-middle Triassic, the lower-middle Jurassic and the upper Jurassic-lower Cretaceous strata, which are confined by three unconformities. The extent to which the formation was eroded differs in different "buried hills" of the Huanghua Depression, indicating that the whole Cretaceous can be lost somewhere, e.g. the "Wmy buried hill".

As shown in Fig. 2, the potential reservoirs consist of lower-middle Triassic, lower-middle Jurassic and lower Cretaceous sandstones. It is worthy to mention that upper Triassic, upper Jurassic and upper Cretaceous strata are missing due to aforementioned tectonic events. The Triassic formation is almost entirely composed of red colored mudstone layers with silty mudrock intercalations, which thus cannot be considered as reservoir rocks. The Jurassic formation includes two lithologies, i.e. a lower one consisting of gray mudstone interbedded with thin to moderate thick sandstones and an upper one characterized by thick river related sandstones and mudstones. In some "buried hills" such as the northeastern "Chh buried hill" and the southern "Dg buried hill", coal seams are encountered in the latter succession. The Cretaceous strata are typically made up of thick igneous rocks in its lower part, which is a common phenomenon in the Cretaceous stratigraphy of the whole Bobai Bay Basin. In addition, there exist sizable clastic rocks that formed coeval with the igneous rocks as well as thick mudstone layers that overlay the igneous/clastic assemblages.

The "Wmy buried hill" is located in the southern part of the Huanghua Depression. This "buried hill" forms as an anticlinal structure of which the top was eroded owing to the late Jurassic to early Paleogene uplift. As a consequence, Triassic strata presently remain in the hilltop (but may also be partially eroded) and whereas Jurassic strata occur only on the flank (Fig. 3A). From the structural map (Fig. 3B), faults developed more intensively on the top than the flank of the "buried hill". Nevertheless, some subtle normal or strike-slip faults with little displacement have been identified, which cannot be ignored considering their impact on potential hydrocarbon migration. The Jurassic reservoirs in the "Wmy buried hill" correspond to fluvial facies (Li et al., 1991; Xu and Wang, 2016). As the seismic reflection in Fig. 3A demonstrates, the reflection interfaces of different rock layers with specific wave impedances display parallel or approximately parallel layering, indicating a sedimentary environment with stable hydrodynamics. The present burial depth of the Jurassic reservoirs in the "Wmy buried hill" exceed 5000 m (Fig. 3B), however, most wells do not penetrate through

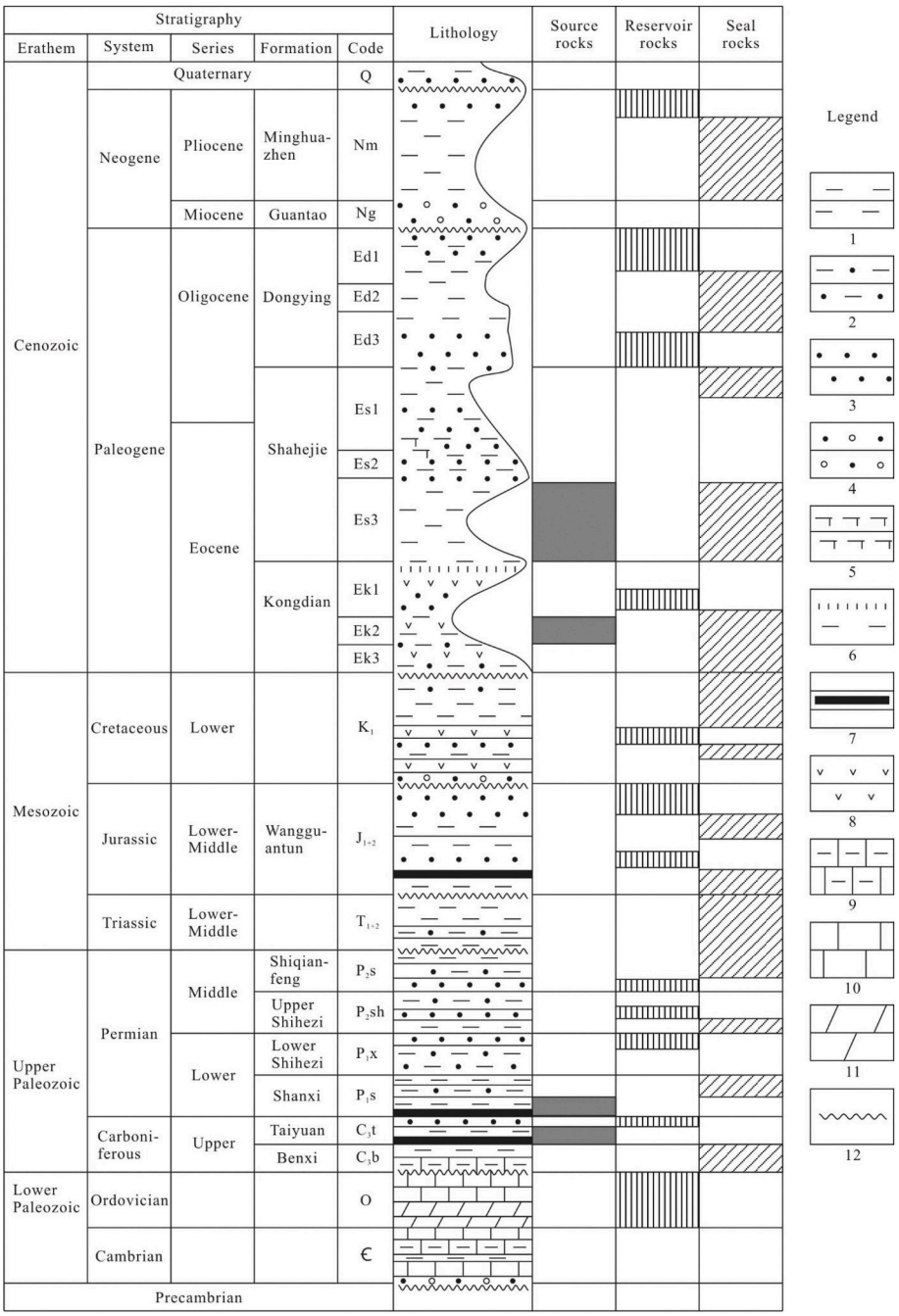

Fig. 2. Generalized Paleozoic-Quaternary stratigraphy of the Huanghua Depression displaying the major petroleum system elements (modified from Zhang et al., 2008).1 = mudstone; 2 = argillaceous sandstone; 3 = sandstone; 4 = sandy conglomerate; 5 = bioclastic limestone; 6 = argillaceous gypsum; 7 = coal seam; 8 = volcanic rock; 9 = argillaceous limestone; 10 = limestone; 11 = dolostone; 12 = unconformity surface.

the Jurassic formation.

3. Samples and methods

Due to the limited exploration of the Jurassic strata in the "Wmy buried hill", cores can only be acquired from 2 wells, i.e. Dc1 and W10. However, the limited cores from W10 all consist of silty mudstone, which is useless from reservoir point of view. Hence, meaningful reservoir samples all were taken from well Dc1. A geophysical analysis of the 3-dimensional seismic data covering most of the Huanghua Depression was firstly performed to study the reservoir architecture. Based on observations made on the cores of well Dc1, the red and white colored zones in sandstones were inspected in specific intervals. Samples were respectively acquired from these two zones in an attempt to decipher what leads to the zonation in cores. In the meantime, other samples are selected from sandstones without zonation characteristics to find the microscopic difference between these two kinds of sandstones. In total twenty-four samples are selected for petrographic and geochemical analysis. Ten impregnated, 30 μm thick and singly polished thin sections were prepared for petrographic analysis, focusing on mineralogical composition, diagenesis and porosity, aiming to assess the reservoir characteristics. Half area of all thin sections was stained by a solution of alizarin red to identify calcite. The petrographic analysis was performed on these thin sections using a Zeiss microscope. Five pre-processed oil-free samples were used for cathodoluminescence analysis. It was performed with a CITL M4 TORNADO microscope and was

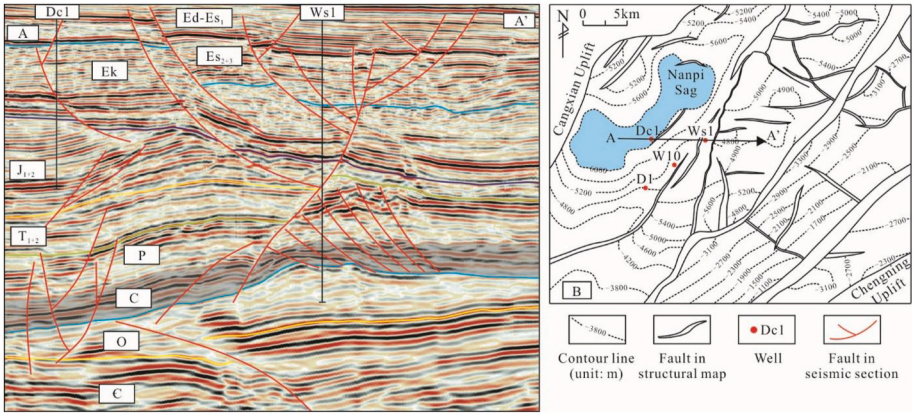

Fig. 3. (A) Seismic section across Wells Dc1 and Ws1 showing an anticlinal structure, the top of which was cut by the unconformity between Jurassic and Paleogene. Є, O, C, P, T, J are codes of Cambrian, Ordovician, Carboniferous, Permian, Triassic and Jurassic, respectively, Ek = Paleogene Kongdian Formation, Es2+3 = the second and third members of the Paleogene Shahejie Formation, Ed = the Paleogene Dongying Formaiton,Es1 = the first member of the Paleogene Shahejie Formation; (B) Structural map of the C–P top of the "Wmy buried hill" in the Hunghua Depression (modified from Zhou et al., 2019). The straight line with an arrow shows the location of the seismic section (A – A′) in Fig. 3A. The blue area represents the Nanpi sag that was proved to hold effective source rocks by explanation. (For interpretation of the references to color in this figure legend, the reader is referred to the Web version of this article.)

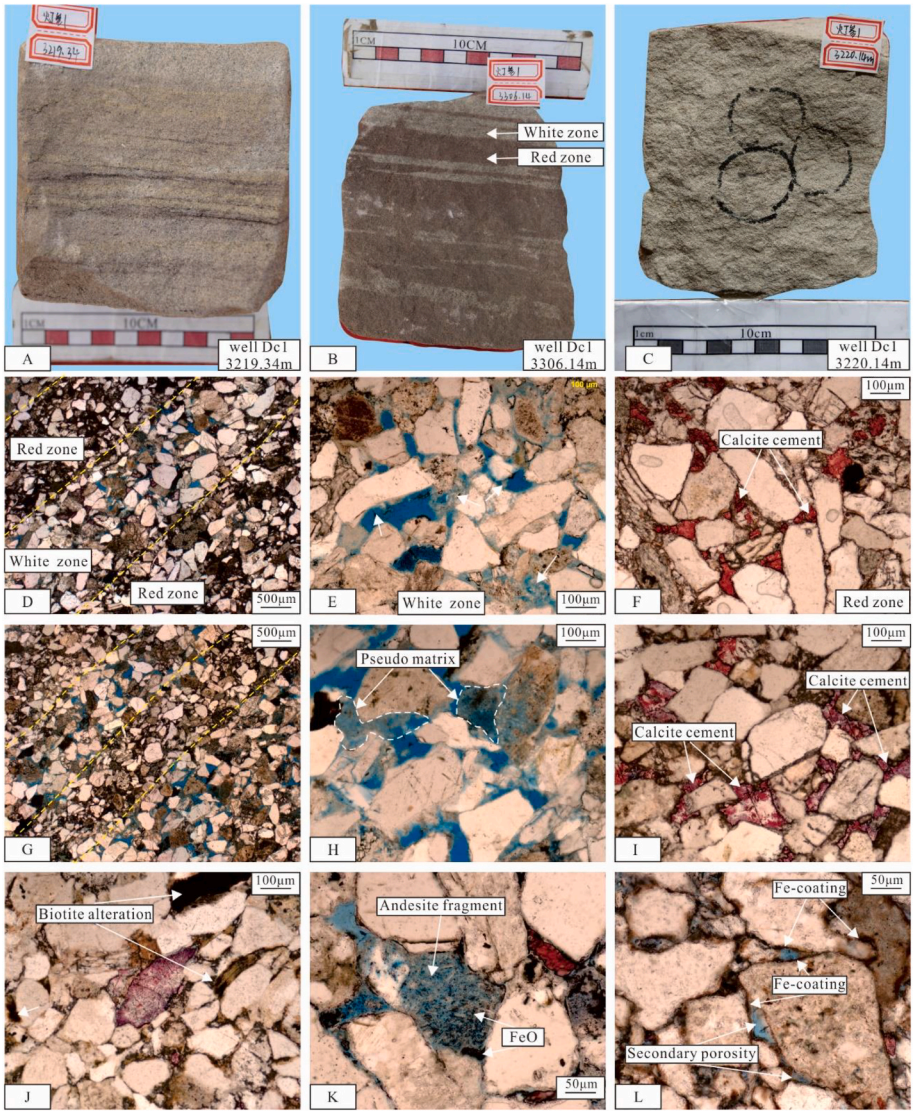

Fig. 4. Characteristics of cores and corresponding photomicrographs taken under transmitted light. Blue in D to L corresponds to porosity. (A) Parallel layered fine-grained sandstone, 3219.34 m, well Dc1. (B) Parallel layered fine-grained sandstone, 3306.14 m, well Dc1. (C) Massive bedded fine-grained sandstone, 3220.14 m, well Dc1. (D) Microphotograph of sample B. Porous and tight zones correspond to white and red zones, respectively. (E) Magnified field of porous zone in Fig. 4D. Feldspar and volcanic rock fragments display moderate dissolution in the porous zone. (F) Magnified field of tight zones in Fig. 4D. Red stained calcite strongly filled the intergranular porosity in the tight zone. (G) Microphotograph of sample C, Well Dc1. Porous and tight zones alternate in massive sandstone without zoning. (H) Magnified field of the porous zone in Fig. 4G. Feldspar and volcanic rock fragments display intense dissolution, giving rise to pseudo matrix, which was intensively compacted, deformed and filled in pores. (I) Magnified field of the tight zone shown in Fig. 4G. Red stained calcite strongly cements intergranular porosity characteristic for the tight zone. (J) In-situ alteration of biotite phases with iron oxide formation, tight zone, 3220.39 m, well Dc1. (K) Iron oxide from andesite fragments alteration, very close to tight zone, 3306.14 m, well Dc1. Black opaque iron-rich minerals "float" on the grain. (L) Fe-coating from altered biotite phases, tight zone, 3306.14 m, well Dc1. Interior of biotite was dissolved to form small-sized secondary porosity. (For interpretation of the references to color in this figure legend, the reader is referred to the Web version of this article.)

especially helpful to study the carbonate diagenetic overprinting. Terrigenous components mainly consisted of quartz, feldspar, volcanic debris, biotite and argillaceous matrix. For addressing the diagenesis, attention went to compaction, dissolution and cement development especially carbonate cementation. These features were compared between the "red" and "white" zones and the sandstones without zones. The latter subsequently will be placed into the burial history of the study area modelled by 1-D module on the BasinMod software platform.

Table 1
Detrital composition of tight and porous zones. TZ = Tight zone, PZ=Porous zone. Rock fragments mainly include volcanic fragments. Biotite phases were commonly altered to iron-rich minerals, the latter are counted as biotite components.

Depth (m)	Type	Quartz (%)	Feldspar (%)	Rock fragment (%)	Biotite (%)	Clay matrix (%)	Calcite content (%)	Average grain size/mm
3219.44	TZ #1	27.8	39.9	11.4	7.8	4.2	8.8	0.13
	PZ#1	41.0	54.1	3.7	0.2	0.8	0.2	0.18
	TZ #2	31.8	36.9	14.3	9.3	0.9	6.8	0.12
	PZ#2	44.0	49.4	4.3	1.0	0.9	0.4	0.25
3219.87	TZ #1	29.4	36.4	9.5	6.9	6.1	11.7	0.13
	PZ#1	44.1	49.9	4.2	0.2	0.4	1.2	0.22
	TZ #2	31.0	42.7	10.6	10.4	1.8	3.3	0.09
	PZ#2	39.7	52.1	5.6	1.8	0.6	0.2	0.23
3220.14	TZ #1	31.8	40.5	10.2	4.7	2.1	10.8	0.1
	PZ#1	36.7	54.8	6.6	0.3	0.8	0.8	0.24
	TZ #2	29.9	34.6	13.1	8.1	5.0	9.3	0.12
	PZ#2	43.1	51.3	4.3	0.5	0.5	0.3	0.24
3306.14	TZ #1	32.4	43.1	7.5	6.1	2.9	8.0	0.12
	PZ#1	39.0	54.5	4.6	0.9	0.5	0.5	0.22
	TZ #2	28.9	41.0	13.8	5.9	5.3	5.1	0.14
	PZ#2	39.2	53.3	5.4	1.1	0.8	0.2	0.23

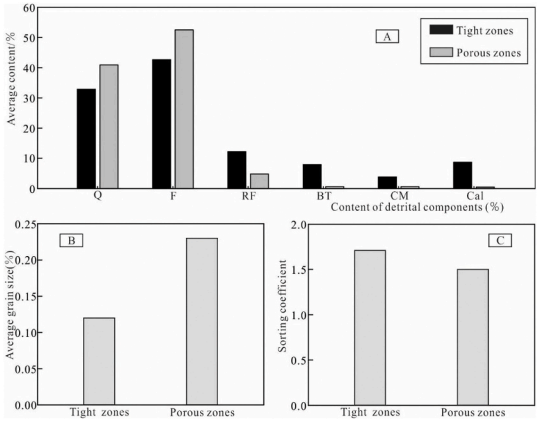

Fig. 5. (A) Average content of detrital components, (B) average grain sizes and (C) average sorting degrees of porous and tight zones. Q = quartz grain, F = feldspar grain, RF = rock fragment, predominantly volcanic fragments, BT = biotite fragment, CM = argillaceous matrix, Cal = calcite cement.

The petrographic analysis is combined with detailed geochemical analysis based on XRF (X-Ray Fluorescence analysis), EPMA (Electro-Probe Microanalysis) and stable carbon-oxygen isotope analysis to constrain the diagenetic processes. XRF with a BRUKER M4 TORNADO instrument qualitatively analyzes the main elemental composition of 2 samples, from which potential migration and loss/gain of certain constituents was inferred. EPMA can qualitatively or quantitatively be utilized to indicate the probable origins of the authigenic minerals based on major and trace element composition (Bouch et al., 2002; Liu et al., 2018; Rath et al., 2011). In this research, quantitative statistics obtained through EPMA from carbonate minerals of the two types of zones were collected. Combined with the CL results, the questions whether carbonate cement within the two color zones are of an identical origin and what its potential origin is, were addressed. The instrument JXA-8230 with working voltage of 15 kV, accelerated current 20 nA and an optional beam spot 1~5 μm was used. In order to assess the origin of the carbonate cement, stable carbon-oxygen isotopes are measured on a Finnigan MAT 253 isotope ratio mass spectrometer. The system provided a precision within ±0.06‰ for carbon and ±0.08‰ for oxygen stable isotopes. Carbon isotope data are reported in "δ" notation in parts per mille relative to the Pee belemnite (PDB) standard and oxygen relative to the Standard Mean Ocean Water (SMOW) as well as the Pee belemnite (PDB). Finally, combined with the burial and thermal histories of the Jurassic reservoirs, the petrographic, diagenetic and geochemical information was systematically used to reconstruct the paleo-fluid flow and reservoir modifying processes of these Jurassic clastic rocks.

4. Results

4.1. Seismic reflection characteristics

As is recognizable in Fig. 3A, the formation on the flank displays a parallel or subparallel seismic reflection configuration, indicating that the clastic rocks display a stable and homogeneous spatial distribution, which reflects a quite large-sized reservoir system. Almost all Mesozoic formations were eroded at the hilltop from the late Jurassic till early Paleocene, forming a time gap corresponding to more than 100 Ma. The Paleogene strata that were deposited after the long-term uplift upon the Jurassic succession, marks an unconformity between the Mesozoic and Cenozoic. With the flank strata of the "buried hill" occurring as homoclinal layers, an apparent angle of approximate 20° exists.

4.2. Petrographic characteristics

The sandstones show typical parallel bedding (Fig. 4A and B) and/or blocky structure (Fig. 4C) with no evident vertical change in grain size at least not on the scale of the studied cores at the depth intervals from 3218.06 to 3223.56 m and 3302.17–3308.55 m. As mentioned above, in certain depth intervals, there exist two types of zones with different colors, namely red and white colored zones, as for example, at the depth of 3306.14 m in well Dc1 (Fig. 4B). The white zones almost do not react with hydrochloric acid, whereas the red zones react quite intensively. From thin section observations, a common feature is that all strata are composed of porous and tight zones (Fig. 4D–I). This exists in both the cores displaying the two kind of zones (Fig. 4B) and cores without color zoning (Fig. 4C). In the cores with alternating colors (e.g. Fig. 4B), the white zones correspond to the porous zones while the red zones reflect the tight zones as observed in thin sections. In tight zones, a considerable amount of iron oxide/hydroxide minerals occurs, causing the tight zones colored red. They display two types of occurrences for Fe-rich minerals namely (1) attached on biotite and andesite fragments as grains (Fig. 4J and K), and as (2) Fe-coatings (Fig. 4L).

It seems like sedimentation controls the formation of porous and tight zones because some evident difference in detrital components exists between both. Quantification of the areas occupied by individual phases (such as terrigenous quartz, feldspar, volcanic rock fragments, biotite, argillaceous matrix, calcite cement as well as porosity) using the Image-Pro Plus software (Wang et al., 2019), allows to compare the contents of the main phases between red and white zones. It should be pointed out that pseudo matrix was classified as terrigenous debris in the

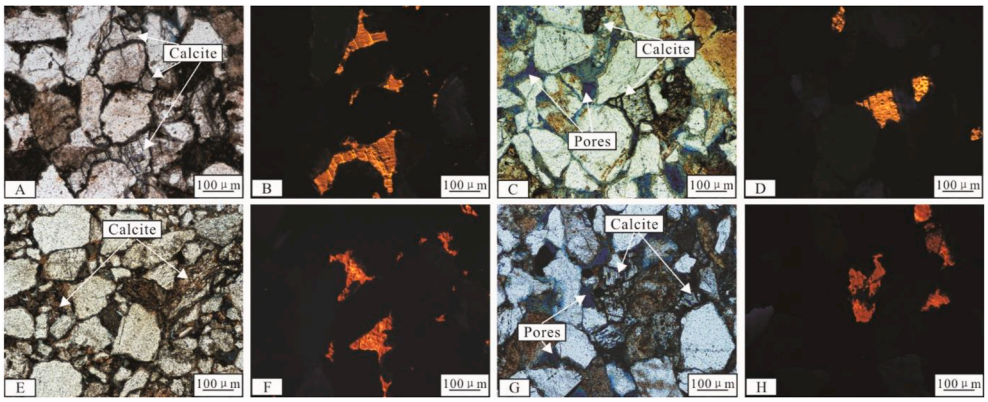

Fig. 6. Transmitted light and cathodoluminescence (CL) images of calcite cement in porous and tight zones with calcite cement displaying an orange luminescence. (A), (B), (C) and (D) 3219.87 m, well Dc1. (E), (F), (G) and (H) 3220.14 m, well Dc1. (For interpretation of the references to color in this figure legend, the reader is referred to the Web version of this article.)

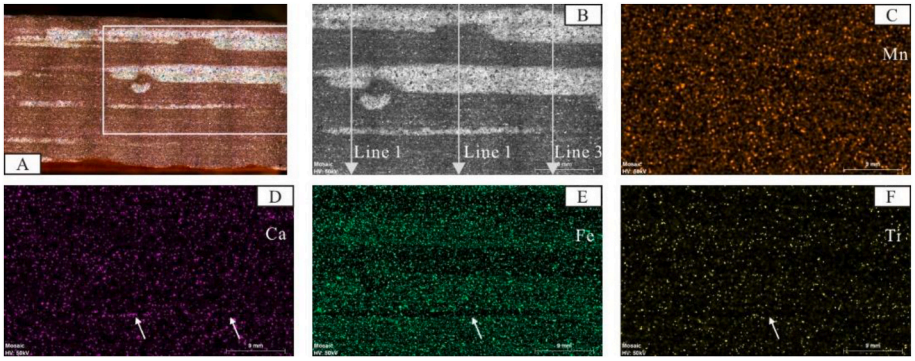

Fig. 7. Distribution of some main elements of a core from a depth of 3306.14 m, well Dc1, examined by X-ray Fluorescence. (A) Original core sample, the area delineated by a white frame corresponds to the region analyzed including white and red zones. (B) Mosaic picture displaying the point locations of analyzed elements. (C)–(F) distributional pictures of Mn, Ca, Fe and Ti. (For interpretation of the references to color in this figure legend, the reader is referred to the Web version of this article.)

calculation. Subsequently, the area of each irregular grain was regarded as a circle, whereby the diameter was calculated by the areal equation of circles. Then, the average circular grain diameters of porous and tight zones can be obtained. Detrital components are displayed below in Table 1. Four samples with typical color zonation were selected, from each of which 2 porous and 2 tight zones were chosen. The result is that the content of quartz and feldspar in porous zones is higher than that in tight zones. In contrast, ductile components, i.e. biotite and clay matrix are much less. Calcite cement is the dominant authigenic component, which shows higher content in tight zones (Fig. 5A). The average grain sizes of the two zones are obviously different, which are much coarser in porous zones (Fig. 5B). In addition, porous zones display better sorting than tight zones, making the interior texture more effective to hold higher permeability.

Diagenetic characteristics also differs in the two zones (Fig. 4D–I) namely: (1) Tight zones are intensely compacted showing that all biotite phases are deformed and grain contacts are tight. Apart from detrital clay matrix, a considerable amount of biotite phases exists as pseudo matrix, which negatively affects the permeability due to its fine size and high content (Fig. 4F and I). In the porous zones, compaction is less apparent. Many rigid grains including quartz and feldspar display point to point contacts. Pressure solution phenomena are absent at the contact points. Some pseudo matrix related to the alteration of volcanic fragments and feldspars developed, which display obvious dissolution features (Fig. 4E and H). (2) Secondary porosity is rarely observed in the tight zones at present, nevertheless, dissolution of feldspar and volcanic fragments should have occurred because calcite partly cemented inside these grains (Fig. 4F and I). Porous zones display a high porosity due to massive development of secondary porosity originating from dissolution of feldspars and/or volcanic fragments. Furthermore, a certain amount of small sized primary pores still exists (Fig. 4E and H). (3) Aside from the intense compaction, calcite cementation is another important process causing porosity reduction. Almost all remaining primary pores in the tight zones were cemented by calcite, which made the reservoir ineffective for oil storage (Fig. 4F and I). On the contrary, porous zones are quite weakly cemented, furthermore it is notable that dissolution of calcite cement did not occur here (Fig. 4E and H). As shown in Fig. 6, calcite cement in either tight or porous zones displays a similar orange cathodoluminescence, supporting involvement of the same fluid inducing calcite cementation.

4.3. Geochemical characteristics

4.3.1. X-ray fluorescence analysis

In the core picture shown in Fig. 7A, an alternation of white and red zones which correspond to porous and tight zones, respectively, is visible. In Fig. 7B, the area for XRF scanning and transects named Line 1, 2 and 3 along which elements are quantitatively analyzed, are illustrated. From Fig. 7C to 7(F), it can be observed that the Mn-content is almost equal in both zones in Fig. 7C, however, the content of Ca, Fe and Ti are lower in the white porous zones than that in red tight zones. In Fig. 7D, the content of Ca is lower in the white zones, however, some small-scale areas in the zones are enriched in Ca as indicated by arrows. Iron displays evident lower concentrations in white zones and higher contents in red zones as shown in Fig. 7E. Biotite and volcanic fragments contain high iron content. When dissolution happened in the reducing condition, Fe is released into the solution and subsequently transferred. The characteristics of Ti is not as apparent as Fe, but still follows the same rules, i.e. the Ti content is less in white zones than that in red zones. In order to analyze the degree of variation of aforementioned elements more clearly, quantitative data from three transects of the core in Fig. 7B was obtained. As is expected, the content distinction of

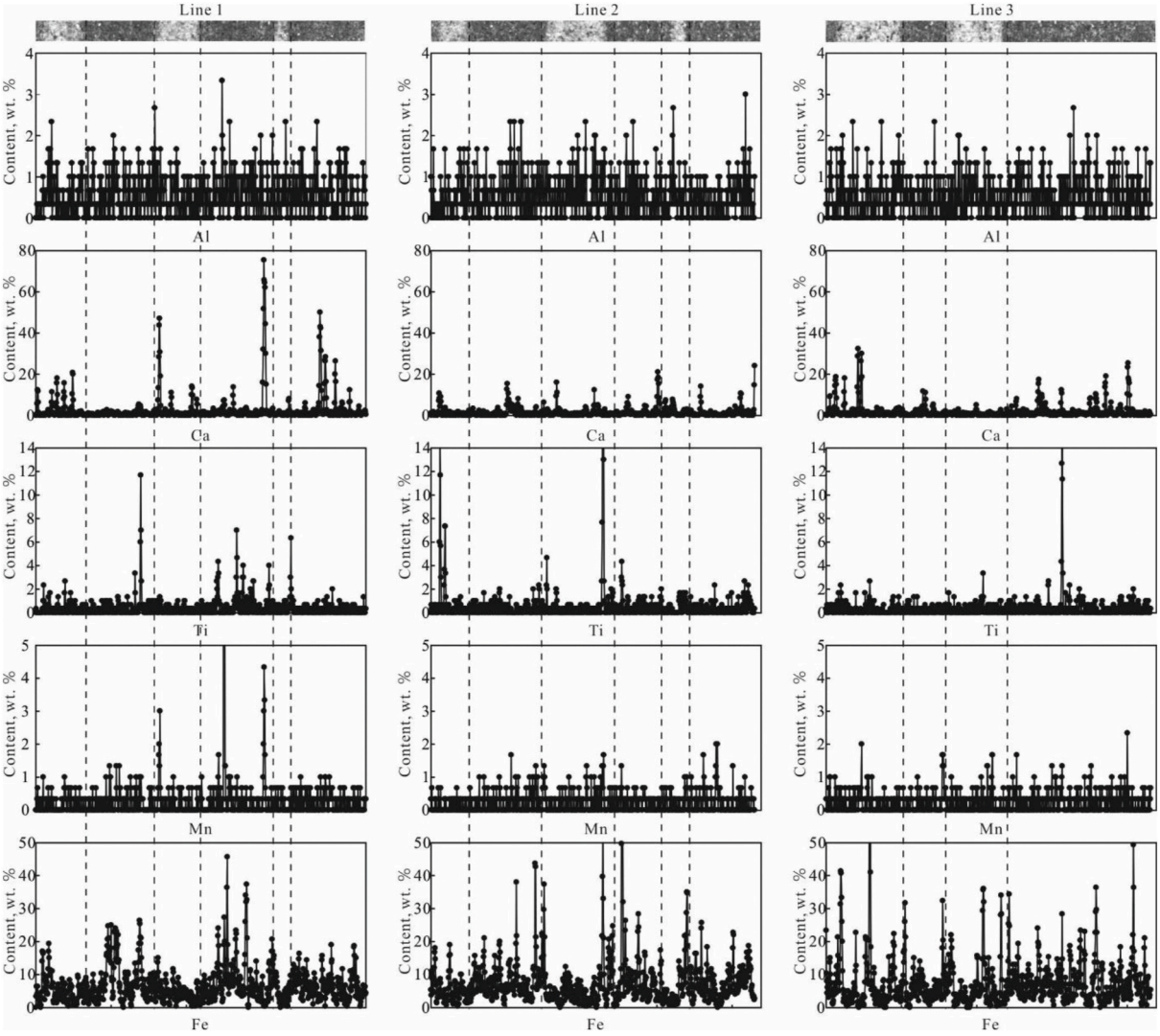

Fig. 8. (A) Content of main elements from three transects in core example at depth of 3306.14 m, well Dc1. The location of the transects are indicated in Fig. 7(B).

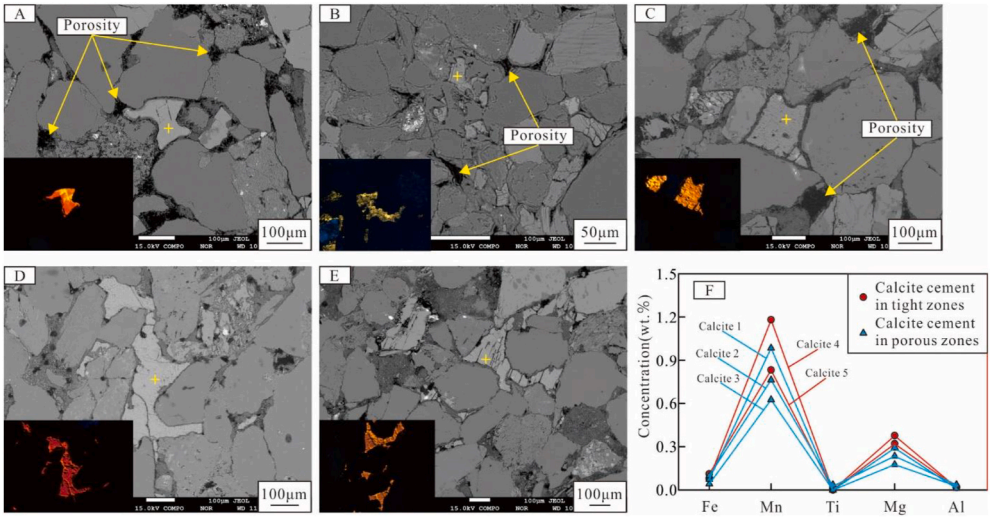

Fig. 9. EBS and corresponding CL photomicrographs (at the bottom left) of calcite cement in primary pores in porous zones and tight zones. (A) Calcite 1, 3220.14 m, well Dc1; (B) Calcite 2, 3306.14 m, well Dc1; (C) Calcite 3, 3219.87 m, well Dc1; (D) Calcite 4, 3220.14 m, well Dc1; (E) Calcite 5, 3219.87 m, well Dc1; (F) Major element composition of the two kinds of calcite cement.

Table 2
Chemical composition of calcite cement developed in porous and tight zones. Content of elements are in weight percentage "wt.%".

Type of cement	Location	CL color	FeO/wt.%	MnO/wt.%	TiO_2/wt.%	MgO/wt.%	Al_2O_3/wt.%	Fe/Mn Ratio
Calcite 1	Porous zone	Orange	0.07	0.98	0	0.18	0.03	0.08
Calcite 2	Porous zone	Orange	0.1	0.76	0.03	0.24	0.04	0.13
Calcite 3	Porous zone	Orange	0.04	0.63	0	0.29	0.01	0.07
Calcite 4	Tight zone	Orange	0.08	1.18	0	0.32	0.02	0.07
Calcite 5	Tight zone	Orange	0.11	0.83	0	0.38	0.02	0.13

Table 3
Carbon-oxygen stable isotopes of calcite cement in the Jurassic sandstones in the "Wmy buried hill". Isotope data are in parts per mill. Precipitation temperature was calculated based on two selected water compositions relative to V-SMOW standard for the O isotope.

Well name	Depth (m)	$\delta^{13}C$, ‰ (V-PDB)	$\delta^{18}O$, ‰ (V-PDB)	$\delta^{18}O$, ‰ (V-SMOW)	Precipitation temperature ($\delta^{18}O_{Pore\text{-}water}$ = −7‰)	Precipitation temperature ($\delta^{18}O_{Pore\text{-}water}$ = −10‰)
Dc1	3219.44 m	−4.4	−13.4	17	48	32
Dc1	3219.87 m	−4.0	−15.0	15.5	58	40
Dc1	3220.14 m	−3.4	−16.5	13.9	69	49
Dc1	3306.44 m	−2.3	−14.6	15.8	56	38

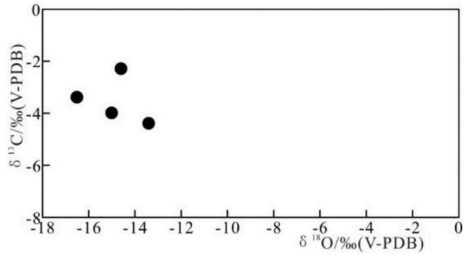

Fig. 10. Distribution diagram of C–O stable isotopes of calcite cement of sandstones in well Dc1.

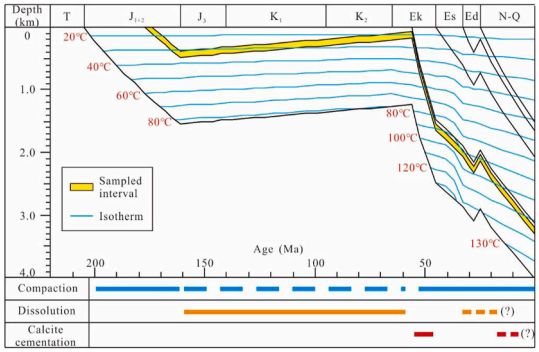

Fig. 11. Burial history and diagenetic sequence of the Jurassic Formation of well Dc1 on the flank of the "Wmy buried hill". T-Triassic, J_{1+2}—Lower to middle Jurassic, J_3—Upper Jurassic, K_1—Lower Cretaceous, K_2—Upper Cretaceous, E—Paleogene, N—Neogene, Q—Quaternary. Note that the sample reservoir interval at depth from 3200 to 3310 m develops in close proximity to the unconformity surface between Mesozoic and Cenozoic.

different elements (see Fig. 8) is in accordance with what is displayed in Fig. 7

4.3.2. Electron Probe Microanalysis

Analyzed points are from pure calcite cement without cleavages that developed both in white (Fig. 9A) and red zones (Fig. 9B), which in both zones displayed saffron or orange luminescence (Fig. 6), which likely reflect low Fe/Mn ratio (Frank et al., 1982). Actually, this ratio varies from 0.07 to 0.13 based on EPMA data. Several characteristic elements such as Fe, Mn, Ti, Mg and Al were selected to deduce the calcite chemical composition (Table 2, Fig. 9).

All analyzed locations displayed high Mn and Mg contents besides low content of Fe, Ti and Al. In general, the distributional characteristics of analyzed elements displayed similar concentrations in porous and tight samples (Fig. 9C). Combined with the nature of the CL characteristics, the calcite cement probably reflects a similar origin. Hence, it can be speculated that the calcite cement in porous and tight zones formed almost contemporaneously. Regarding the diagenesis of the two zones, the paragenesis are alike, i.e. with the following sequence: compaction-dissolution of unstable detritus-calcite cementation. As observed from microscopy, calcite precipitated not only in secondary porosity deriving from dissolution of volcanic fragments and feldspars, but also in quite small-sized primary pores indicating that calcite precipitation postdated considerable compaction.

4.3.3. Carbon and oxygen stable isotopes

Samples which are selected for C–O stable isotope analysis are all from well Dc1, and the calcite analyzed has a mixed origin since it was coming from both porous and tight zones. The $\delta^{18}O$ values of the calcite cement ranges from −16.5 to −13.4‰(PDB) based on four samples, with an average of −14.9‰ and the $\delta^{13}C$ values ranges from −4.4 to −2.3‰ (PDB) with an average of-3.5‰(PDB) (Table 3, Fig. 10).

5. Discussion

5.1. Indication of the unconformity

When investigating the rock-fluid interactions in clastic sandstones from Shengtuo area in Dongying sag and Gaoliu area in Nanpu sag in the Bohai Bay Basin in northeastern China, Yuan and collaborators identified two types of diagenetic systems i.e. open and closed systems. The open system in Gaoliu area was tightly related to an unconformity that was caused by the tectonic uplift at the end of Paleogene (Yuan et al., 2015a, 2015b), which allowed the sandstones to suffer from meteoric freshwater leaching, leading to the dissolution of feldspars whereby dissolved composition were removed from the reservoirs. Hence, authigenic clay such as illite, kaolinite and quartz did not substantially develop in these sandstones. There is a similar geological setting between Gaoliu area and the "Wmy buried hill" with respect to formation

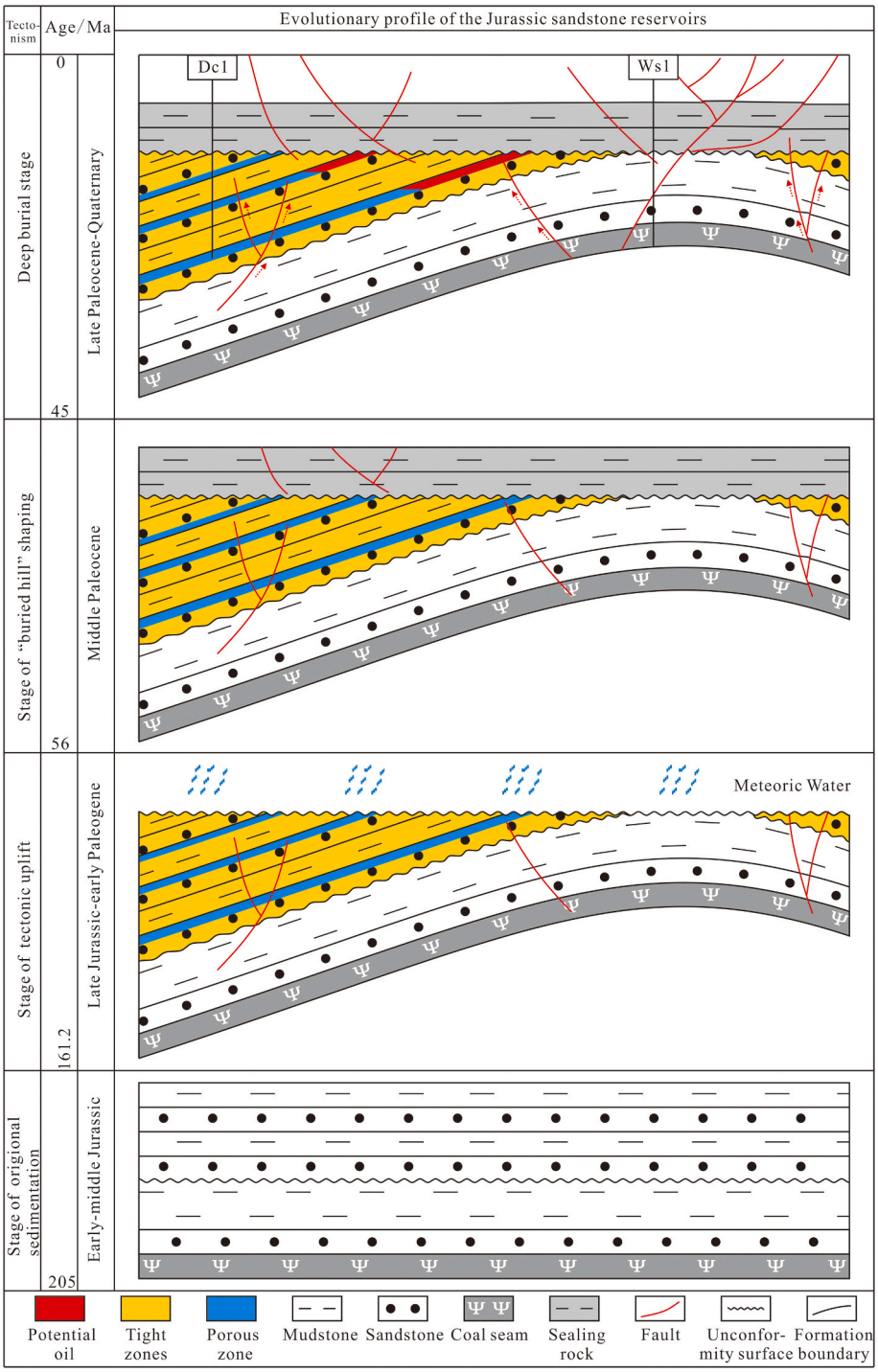

Fig. 12. Evolutionary history of the Jurassic sandstone reservoirs in the "Wmy buried hill". It is noteworthy that thickness of the porous zones is not that large as illustrated, which is mainly aimed to demonstrate that porous zones are layer-like and alternating with tight zones in the sandstone reservoir.

Table 4
Calculation of amount of porous/tight zones in cored intervals. PZ = porous zones, SI = sandstone interval.

Core color	Well	Depth range (m)	Thickness of PZ (m)	Thickness of SI (m)	Rate of PZ/SI (%)
Zonation	Dc1	3305.15–3307.25	0.56	2.1	~26
Non-zonation	Dc1	3218.06–3220.45	0.71	2.39	~30

of the unconformity. When the parallel formation was uplift angularly, the meteoric water, although depends on the permeability of the reservoir below the unconformity surface, must have capability, to some degree, to penetrate downwards from the relatively tectonic highs when derived by gravity. Due to the heterogeneity of the stratigraphic configuration, it is possible for the products originated from dissolution

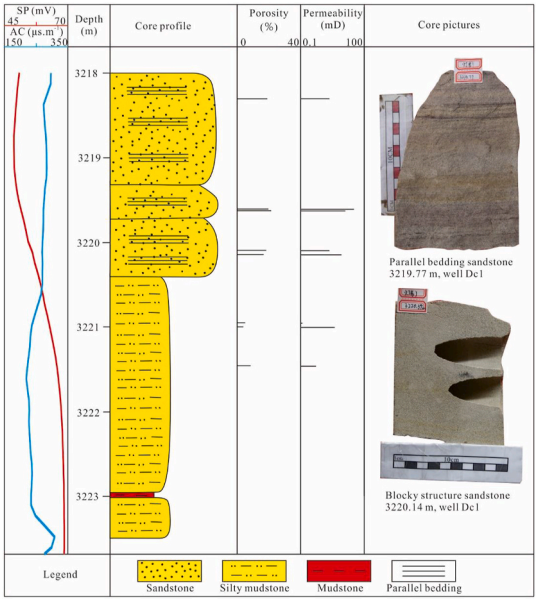

Fig. 13. Petrographic and petrophysical characteristics of the first cored rock interval, well Dc1. AC = acoustic time difference curve, SP = self-potential. Porosity and permeability are present-day measured values.

of terrigenous components to migrate at a certain distance. In the studied Jurassic sandstones in the "Wmy buried hill", neither authigenic kaolinite nor illite were observed although the amount of the secondary porosity derived from dissolved volcanic fragments and feldspars is high. Hence, it can be deduced that the dissolved products did not stayed in the diagenetic system, which indicates an open system whereby the obvious angular unconformity can act as evidence for the development of early meteoric diagenesis.

5.2. Evidence of meteoric freshwater leaching

Selective dissolution gave rise to the white zones in reservoirs, which is different from the general opinion that the white zones in thick clastic rocks originate from intensive carbonate cementation and most commonly calcite cementation (Ma et al., 2016, 2019, 2021). From the XRF result, Fe and Ti are apparently present in low concentration in white zones and are present in red zones, which is why the zones are red colored. Compared with the red zones, calcite content in white zones is much less, explaining the weak reaction with hydrochloric acid in the cores. From the high Mn contents via EPMA, the calcite cement likely formed in a suboxic or weakly reductive environment. Such a system is typical for shallow meteoric aquifers which occur already at a certain depth. Ferric iron is difficult to transfer in aqueous solution, hence iron was massively removed from the white zones in the form of Fe^{2+}, indicating a same suboxic or weakly reductive environment as Mn. The smaller grained zones with relatively lower permeability did not allow to leach all the Fe-oxide coatings and the alteration of unstable grains was less effective. This is supported by the poor sorting shown in Fig. 5C as well as a high biotite content in Fig. 5A, which considerably destroy the permeability. Therefore, these lithologies were more affected by burial compaction which additionally lowered the permeability. In the meantime, existence of pseudo matrix originating from volcanic fragments that are vulnerable to acid matters due to the chemically unstable components such as feldspar, hornblende and volcanic glass, explains the early dissolution, because the volcanic fragments are so mechanically rigid to get deformed severely unless they are altered by acid dissolution in advance to cause the reduction of rigidity. Thus, it can be deduced that meteoric freshwater leaching caused volcanic fragments and feldspars dissolution in a suboxic to reductive and acidic fluid system, which was followed by calcite cementation.

Based on former studies (Jansa and Urrea, 1990; Wilkinson et al., 2006) the $\delta^{13}C$ values from marine carbonates commonly are distributed between 0 and 3‰(PDB) and $\delta^{13}C$ values of carbonate phases derived from meteoric freshwater vary between −1 and −5‰(PDB), while $\delta^{13}C$ values of organic origin are more negative and often varies around −25‰(PDB). Friedman and O'Neal (1977) proposed an equation for calculating the formation temperature of calcite precipitation in a calcite-water fluid system. Due to such fine grains in the sandstones, efforts put into finding fluid inclusions in the calcite cement have failed, thus the data from previous researchers are used here. The $\delta^{18}O$ values representing meteoric water range around −7‰, in addition, the values could vary along with water temperatures (Bath et al., 1987; Schmid et al., 2004). Whereby, the formation water temperature of calcite cement would vary between 48 and 69 °C. The $\delta^{18}O$ of the present formation water in the Bohai Bay Basin that the "Wmy buried hill" is located in, ranges approximately from −10‰~-8‰ (VSMOW) (Sun et al., 1982; Song et al., 2006). Taking −10‰ (VSMOW) as original $\delta^{18}O$ of the pore water, the estimated temperature for the calcite precipitation would vary between 32 and 49 °C (Table 3). On the basis of the diagenetic sequence, calcite cementation occurred in the early Paleocene within a shallow burial or early post-depositional setting.

From the data and well logs of the two wells penetrating the Jurassic Formation in the "Wmy buried hill", they do not display any petroleum shows. Most faults develop at the top of the "buried hill" where Jurassic strata were partially eroded. Whereas faults development was clearly less on the flank of the "buried hill" particularly adjacent to well Dc1. It can be speculated that reservoir diagenesis in well Dc1 was weakly affected by organic matter from underlying or overlying source rocks (Zhao et al., 2018). Hypothetically, if potential hydrocarbons affected the precipitation of the calcite cement, the signature of the organic matter from kerogen maturation will possess rather negative $\delta^{13}C$ values (Surdam et al., 1984, 1989), which could reach −25‰ (VPDB). Meanwhile, the reductive fluid bleached the red sandstone to form white porous zones in the coarser grained laminae. In addition, the dissolved constituents including clay minerals and authigenic quartz would precipitate almost in situ due to the sealing of lateral Triassic mudstones and lower Paleogene mudstones underlying the unconformity surface between Mesozoic and Cenozoic strata. Nevertheless, all data such as $\delta^{13}C$ signature and element composition of calcite cement do not support an organic origin but display a close relationship with carbon dioxide carried by meteoric water.

Cementation discrepancy between these two types of zones apparently displayed that nucleation is different. Due to the low original maturity degree of tight sandstones, meteoric water was weakened on removing the nucleation sites that stimulated later calcite cementation. In contrast, calcite merely partially participated in that most nucleation sites were migrated out of the system. Hence, original sedimentary conditions not only play a key point in the diagenetic modification of new sediment but also in the ancient strata, Jurassic here.

5.3. Evolution of reservoir modification

From the burial and thermal history diagram reconstructed by the use of BasinMod Basin Simulation software, long-term meteoric water leaching could have occurred in a period from the late Jurassic to early Paleogene thus representing a time duration of more than 100 Ma. Later, the Jurassic formation was rapidly deeply buried (Fig. 11). Due to the uplift movement, it is even uncertain whether the upper Jurassic – Cretaceous sediments were even deposited in the "Wmy buried hill" (Zhang et al., 2019). In Fig. 11 we combined the diagenetic evolution with the burial history.

Taking all data together, the sandstone reservoirs on the flank of the "Wmy buried hill" were affected by meteoric water leaching which caused dissolution of unstable mineral and volcanic detritus phases to form porous zones in sandstone reservoirs with 3.9%–21.3%present-day

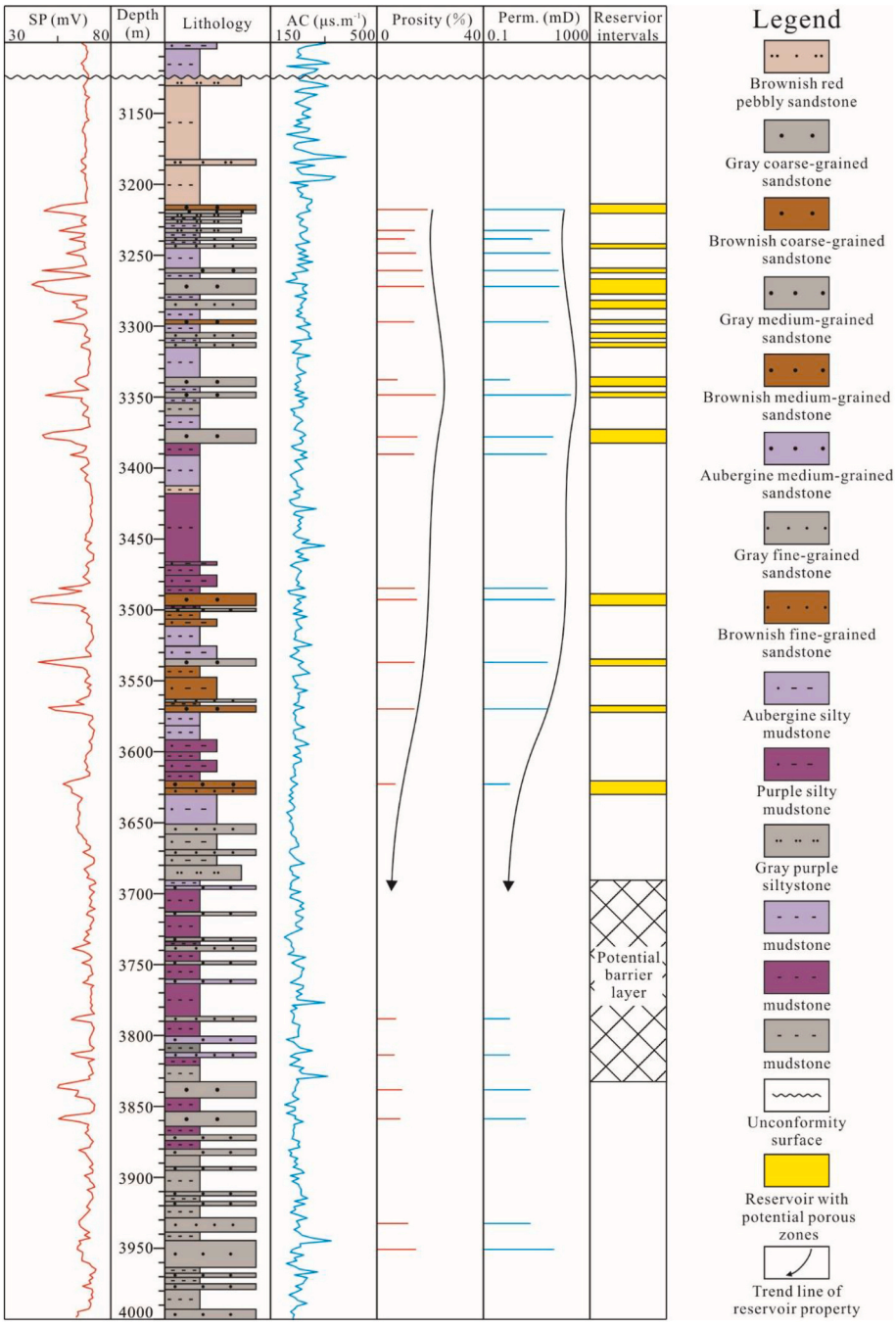

Fig. 14. Identification and distribution of sandstone intervals in whole well profile, well Dc1. Porosity and permeability data are from well logging interpretation.

porosity (averaging 12.0%), which is predominantly secondary porosity. Considering the diagenesis as well as the burial and thermal history, the reservoir evolution can be divided into four stages. At the first stage from 205 to 161.2 Ma, the lower-middle Jurassic sandstones were deposited and underwent some burial. The sedimentary environment was quite arid and rich in oxygen, leading to abundance of iron oxide/hydroxide to form massive red sandstones. The second stage corresponds to the period when the strata was uplifted and folded to form an anticlinal structure. The Jurassic suffered from long-term uplift from 161.2 to 56 Ma lasting approximate 100 Ma. On the top of the buried hill, the Jurassic formation was severely eroded until the Triassic outcropped whereas on the flank the Jurassic formation was partly preserved with a thickness of over 1000 m, forming the present-day reservoirs. During the uplift, meteoric water penetrated into the Jurassic sandstones due to the surface weathering at the top of Jurassic strata. The coarser sandstones, with higher remaining primary porosity and permeability, were more prone to dissolution creating quantities of secondary pores and some bleaching took place due to interaction with suboxic to reducing meteoric fluids. By contrast, the finer grained sandstones corresponding to the red zones, were less evidently affected by dissolution also due to their smaller grain size and higher degree of physical compaction. Meanwhile, during the folding movements, small-scale faults affected Jurassic reservoirs and underlying upper Paleozoic coal-measures (Fig. 3A, the gray colored zone). At the third stage during the early Paleogene, the Kongdian Formation containing source rocks in its middle part was deposited. The meteoric water with dissolved CO_2 supplied calcium to form the calcite in both white and red zones. Volcanic fragments can release a mass of Ca^{2+} when dissolved, serving as

Table 5
Log porosity and permeability statistics and their relationship with the unconformity surface between the Mesozoic and the Cenozoic strata. The depth of the unconformity surface is 3,126 m.

Original Interval No.	Top depth (m)	Bottom depth (m)	Middle depth (m)	Distance from the unconformity surface (m)	Porosity (%)	Permeability (mD)
39	3214.5	3221.1	3217.8	91.8	19.07	111
40	3230.8	3234	3232.4	106.4	14.33	30
41	3237.6	3239.6	3238.6	112.6	10.53	7
42	3247.1	3249.8	3248.45	122.45	14.7	33
43	3258.9	3262.6	3260.75	134.75	17.19	68
44	3266.6	3277.6	3272.1	146.1	17.72	72
45	3295.6	3298.3	3296.95	170.95	14	28
46	3337.4	3338.3	3337.85	211.85	7.71	1
47	3346.5	3350.3	3348.4	222.4	22.12	194
48	3373.4	3382.6	3378	252	15.15	42
49	3389.6	3391.1	3390.35	264.35	14.01	24
50	3483.3	3486.3	3484.8	358.8	14.25	26
51	3488.6	3496.8	3492.7	366.7	15.11	49
52	3534.6	3539.5	3537.05	411.05	14.11	26
53	3567.6	3571.8	3569.7	443.7	14.08	26
54	3620.4	3625.3	3622.85	496.85	6.87	1

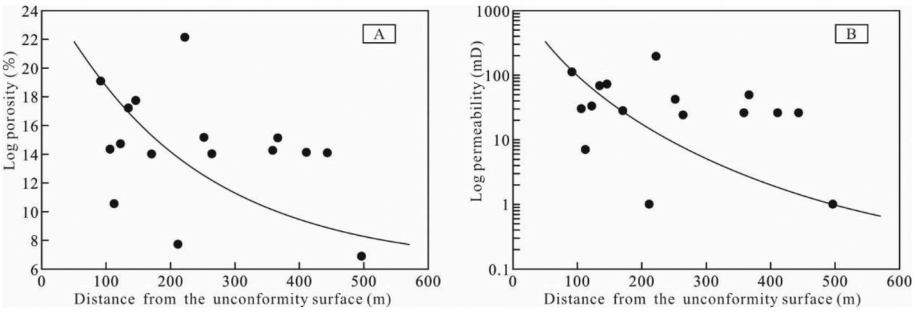

Fig. 15. Crossplots of distance from the unconformity surface versus log porosity (A) and permeability (B) for sandstone intervals.

source of Ca for calcite cement. The difference is that residual Ca content is higher in the red zones due to the low transport velocity for dissolved ions and larger amount of nucleation sites, which is the result of early intense compaction with high content of biotite and clay matrix and high sorting degree. On the contrary, porous zones predominated by secondary porosity became less cemented thanks to the high maturity degree of sandstones and a low amount of Ca-bearing phases that were already dissolved to cause less nucleation sites. Meanwhile, normal faults resulting from stretching stress started to form (Zhang et al., 2008), some of which can penetrate into the Jurassic at the top of the "Wmy buried hill" as is shown in Fig. 3A. The faults can serve as potential pathway of petroleum migration in the deep burial (Zhao et al., 2018). This corresponds with the incipient stage of the "Wmy buried hill". During the fourth stage, as the overlying formation were gradually deposited, the upper Paleozoic coal-measure kerogens reached a high maturity and produced substantial hydrocarbons. The oil and gas condensate pools have successfully been explored and put into production in the Permian sandstone reservoirs of the "Wmy buried hill" (Zhao et al., 2018; Zhou et al., 2019). Thus, it can be hypothesized that the overlying Jurassic reservoirs also can capture migrating hydrocarbons when the effective faults acting as pathways developed during the last stage. At the same time, as the Paleogene formation mainly composed of mudstones were gradually compacted, which formed the upper high-quality sealing layers to prevent petroleum loss upwards (Fig. 12).

5.4. Prediction of reservoir quality

From the comprehensive study including aspects of petrography, petrology and geochemistry, some sandstone reservoirs contain secondary porosity zones, which has potential to accumulate hydrocarbons. Whereas, for a quite large interval of sandstones no cores are available, resulting in the difficulty to qualitatively and/or quantitatively estimate reservoir quality either for the whole well or the entire "buried hill". In order to resolve this, a statistical approach has been worked out, i. e. (1) for the cored sandstone intervals, the rate of porous zones was calculated, (2) calculate the amount of sandstone intervals displaying obvious negative anomalies in Self-potential (SP) log curves in the Jurassic formation of the well, and (3) evaluate the potential total thickness of porous sandstone zones.

Two intervals were cored, i.e. 3218.06–3223.56 m and 3302.17–3308.55 m. The sandstones from these intervals displayed porous and tight zones, the former being potential reservoirs for petroleum accumulation. Through the thickness statistics of white porous zones in the sandstones, their amount can reach up to an average of about 28% considering both cores with zonation and cores without zonation (Table 4). Subsequently, the core, logging and lithological data were put together to determine response of porous sandstones, namely assemblages of porous and tight zones, to the lithological profile and log curves, in order to evaluate the developing degree of the porous sandstones in the whole well. Taking an example from the first interval of cores (Fig. 13), the porous sandstone interval displays a negative anomaly in SP and a positive deviation of AC. Subsequently, all reservoir intervals are identified in the whole well profile (Fig. 14), the total thickness of which can sum up to approximate 88.2 m. At last, combining the rate of porous/tight zones and the thickness of reservoir intervals, the porous reservoir accumulative thickness can be calculated being 25 m (88.2 m multiplied by 28%). It is notable that the accumulated thickness does not include that at depth beyond than 3630 m, although certain sandstones with quite high properties occurred. As such, the argument can be made based on that far from like the marine sandstones that allow meteoric water to flow into the formation until the depth of 2–3 km (Kevin, 1995), terrigenous fluvial sandstones possess relatively poor heterogeneity which is commonly caused by frequent

mudstones intercalation, making it difficult for the meteoric water to go through the strata downwards. In addition, a barrier layer with a thickness about 100 m that mainly consist of mudstones exists, which could be a potential barrier to hinder meteoric water flow (Fig. 14).

Whereas, from the data statistics in Table 5 and the two crossplots shown in Fig. 15, it is obvious that the petrophysical properties get lower as the burial depths increases regardless of the anomalous points at deep depth positions. Thus, the effect of meteoric freshwater leaching on reservoir property enhancement displays decreases with depth, indicating reservoir quality gets poorer which also can be deduced by the gradually weaker negative anomalies in SP curve. In conclusion, among the whole 88.2 m of porous reservoirs, intervals close to the unconformity surface are more effective and significant. Although carbonate destroyed the most primary pores in tight zones and partial ones in porous zones, carbonate phases precipitating in the shallow formation such as aforementioned weathered reservoirs or captured in the deeply buried reservoirs are meaningful to study the CO_2 sequestration (Ma et al., 2020a,b; Zan et al., 2020), which could be the prospective research point.

6. Conclusions

In the Jurassic succession in the "Wmy buried hill" porous and tight sandstones co-exist. The porous zones are coarser grained and possess a low content of volcanic fragments, biotite, calcite cement and a higher porosity. By contrast, the tight zones are on average finer grained, possess a lower porosity and higher content of volcanic fragments, biotite and calcite cement. The distinct diagenetic porosity process relates to the selective leaching of unstable mineral grains by meteoric freshwater. The approximately same composition in calcite cement from the two zones supports a similar origin. The carbon isotope values range from −4.4 to −2.3‰(VPDB) averaging −3.5‰(PDB) and quite low precipitation temperatures calculated through oxygen isotopes supports a meteoric origin of the calcite. In addition, calcite cement does not display dissolution, and locally filled secondary porosity. Hence, the formation of calcite cement postdated dissolution of clastic minerals by meteoric water. The evolution process of the reservoir rocks can be divided into four stages. The second stage is the key period for formation of secondary porosity and faults derived from compressional stress are potential pathways linking the Jurassic reservoirs with underlying coal-measures holding carbonaceous rocks able to generate oil when deeply buried as in stage 4. This last stage is the critical period of petroleum migration and potential accumulation because the thermomaturation of the underlying source rocks produce substantial hydrocarbons and sealing rocks were intensely compacted to prevent hydrocarbons leakage.

Combining the rate of porous zones/reservoir intervals (averaging 28%) and the cumulative thickness (about 88.2 m) of reservoir intervals in the whole well profile, porous reservoirs of approximate 25 m thick can be finally predicted. Furthermore, the upper intervals close to unconformity surface are clearly more effective and significant for prospective exploration.

Credit author statement

Zhukun Wang: Conceptualization, Methodology, Formal analysis, Investigation. Yingchang Cao: Supervision, Project administration. Rudy Swennen: Conceptualization; Methodology, Writing - Review & Editing. Guanghui Yuan: Conceptualization, Formal analysis. Ke Wang: Resources, Data Curation.

Declaration of competing interest

The authors declare that they have no known competing financial interests or personal relationships that could have appeared to influence the work reported in this paper.

Acknowledgements

This study was financially supported by the National Science and Technology Special Grant (No. 2016ZX05006-007) and the China Scholarship Council (CSC).

References

Bath, A.H., Milodowski, A.E., Strong, G.E., 1987. Fluid flow and diagenesis in the East Midlands Triassic sandstone aquifer. Geol. Soc. Londn. Special Public. 34, 127–140.
Bjørlykke, K., Nedkvitne, T., Ramm, M., Saigal, G.C., 1992. Diagenetic processes in the brent group (middle jurassic) reservoirs of the north sea: an overview. Geol. Soc. Londn. Special Public. 61, 263–287.
Bouch, J.E., Hole, M.J., Trewin, N.H., Chenery, S., Morton, A.C., 2002. Authigenic apatite in a fluvial sandstone sequence: evidence for rare-earth element mobility during diagenesis and a tool for diagenetic correlation. J. Sediment. Res. 72, 59–67.
Emery, D., Myers, K.J., Young, R., 1990. Ancient subaerial exposure and freshwater leaching in sandstones. Geology 18, 1178–1181.
Frank, J.R., Carpenter, A.B., Oglesby, T.W., 1982. Cathodoluminescence and composition of calcite cement in the taum sauk limestone (upper cambrian), southeast Missouri. J. Sediment. Res. 52, 631–638.
Friedman, I., O'Neal, J., 1977. Compilation of Stable Isotopes Fractionation Factors of Geochemical Interest US Government Printing Office 440.
Hrabar, S.V., Potter, P.E., 1969. Lower west baden (mississippian) sandstone body of owen and greene Counties, Indiana. AAPG (Am. Assoc. Pet. Geol.) Bull. 53, 2150–2160.
Jansa, L.F., Urrea, V.H.N., 1990. Geology and diagenetic history of overpressured sandstone reservoirs, Venture gas field, Offshore Nova Scotia, Canada. AAPG (Am. Assoc. Pet. Geol.) Bull. 74, 1640–1658.
Kevin, P., 1995. Diagenesis of lower Jurassic sandstone, block 211/13 (Penguin area), UK northern north sea. Mar. Petrol. Geol. 12, 219–228.
Landes, K.K., Amoruso, J.J., Charlesworth, L.J., Heany, F., Lesperance, P.J., 1960. Petroleum resources in basement rocks. AAPG (Am. Assoc. Pet. Geol.) Bull. 44, 1682–1691.
Li, W., Liu, Y., Qu, Z., et al., 1991. Sedimentary characteristics and environment of Jurassic sandstones in South Huanghua depression. Oil Gas Geol. 387–396 (In Chinese with English abstract).
Liu, Y., Hu, W., Cao, J., Wang, X., Tang, Q., Wu, H., Kang, Xun, 2018. Diagenetic constraints on the heterogeneity of tight sandstone reservoirs: a case study on the Upper Triassic Xujiahe Formation in the Sichuan Basin, southwest China. Mar. Petrol. Geol. 92.
Ma, B., Eriksson, K., Cao, Y., et al., 2016. Fluid flow and related diagenetic processes in a rift basin: Evidence from the fourth memberof the Eocene Shahejie Formation interval, Dongying depression, Bohai Bay Basin, China. AAPG Bulletin 100, 1633–1662.
Ma, B., Cao, Y., Eriksson, K., et al., 2019. Carbonate cementation patterns, potential mass transfer, and implication for reservoir heterogeneity in Eocene tight-oil sandstones, Dongying depression, Bohai Bay Basin, China: Evidence from petrology, gechemistry, and numerical modeling. AAPG Bulletin 103, 3035–3067.
Ma, B., Cao, Y., Eriksson, K., 2020a. Microbially induced dolomite precipitates in Eocene lacustrine siliciclastic sequence in the Dongying depression, Bohai Bay Basin, China: Evidence from petrology, geochemistry, and numerical modeling. AAPG Bulletin 104, 2051–2075.
Ma, B., Cao, Y., Zhang, Y., et al., 2020b. Role of CO2-water-rock interactions and implications for CO2 sequestration in Eocene deeply buried sandstones in the Bonan Sag, eastern Bohai Bay Basin, China. Chemical Geology 541, 119585.
Ma, B., Lu, Y., Eriksson, K., et al., 2021. Multiple organic–inorganic interactions and influences on heterogeneous carbonate-cementation patterns: Example from Silurian deeply buried sandstones, central Tarim Basin, north-western China. Sedimentology 68, 670–696.
Meng, W., Chen, Z., Li, P., Guo, Y., 2009. Exploration theories and practices of buried-hill reservoirs: a case from Liaohe Depression. Petrol. Explor. Dev. 36, 136–143.
Powers, S., 1922. Reflected buried hills and their importance in petroleum geology. Econ. Geol. 17, 233–259.
Powers, S., 1926. Reflected buried hills in the oil fields of Persia, Egypt, and Mexico. AAPG (Am. Assoc. Pet. Geol.) Bull. 10, 422–442.
Purvis, K., 1995. Diagenesis of lower jurassic sandstones, block 211/13 (Penguin area), UK northern north sea. Mar. Petrol. Geol. 12, 219–228.
P'An, C.-H., 1982. Petroleum in basement rocks. AAPG (Am. Assoc. Pet. Geol.) Bull. 66, 1597–1643.
Qi, F., Xie-Pei, W., 1984. Significant role of structural fractures in Renqiu buried-hill oil field in Eastern China. AAPG (Am. Assoc. Pet. Geol.) Bull. 68, 971–982.
Ramm, M., 1992. Porosity-depth trends in reservoir sandstones: theoretical models related to Jurassic sandstones offshore Norway. Mar. Petrol. Geol. 9, 553–567.
Rath, A., Exner, U., Tschegg, C., Grasemann, B., Laner, R., Draganits, E., 2011. Diagenetic control of deformation mechanisms in deformation bands in a carbonate grainstone. AAPG (Am. Assoc. Pet. Geol.) Bull. 95, 1369–1381.
Sam Boggs, J., 2006. Principles of Sedimentary and Stratigraphy, fourth ed.
Schmid, S., Worden, R.H., Fisher, Q.J., 2004. Diagenesis and reservoir quality of the sherwood sandstone (triassic), Corrib field, slyne basin, west of Ireland. Mar. Petrol. Geol. 21, 299–315.
Schmidt, V., Mcdonald, D.A., 1979a. The role of secondary porosity in the course of sandstone diagenesis. SEPM Special Publ. 175–207.

Schmidt, V., Mcdonald, D.A., 1979b. Texture and recognition of sedimentary porosity in sandstones. SEPM Special Publ. 26, 209–225.
Song, X., Liu, X., Xia, J., Yu, J., Tang, C., 2006. A study of interaction between surface water and groundwater using environmental isotope in Huaisha River basin. Sci. China Earth Sci. 49, 1299–1310.
Sun, B., Xie, J.S., Li, G.R., 1982. Hydrogen and oxygen isotopic composition and genesis of the ground water in Jizhong Depression. Oil Gas Geol. 3, 253–9985 (In Chinese with English abstract).
Surdam, R.C., Boese, S.W., Crossey, L.J., 1984. The Chemistry of Secondary Porosity. AAPG Memoir, pp. 127–149.
Surdam, R.C., Crossey, L.J., Hagen, E.S., 1989. Organic-inorganic interactions and sandstone diagenesis. AAPG (Am. Assoc. Pet. Geol.) Bull. 73, 1–23.
Tomlinson, C., 1926. Buried hills near Mannsville Oklahoma. AAPG (Am. Assoc. Pet. Geol.) Bull. 10, 1558–9153.
Tong, X., Huang, Z., 1991. Buried-hill discoveries of the Damintun depression in north China. AAPG (Am. Assoc. Pet. Geol.) Bull. 75, 780–794.
Walters, R., 1946. Buried pre-cambrian hills in northeastern Barton County, central Kansas. AAPG (Am. Assoc. Pet. Geol.) Bull. 30, 1558–9153.
Wang, W., Jiang, Y., Yuan, J., Liu, J., Zhang, S., Swennen, R., 2019. Characteristics and migration mechanisms of natural gas in tight sandstone reservoirs in the Longfengshan sag, Songliao Basin, China. J. Petrol. Sci. Eng. 174, 456–467.
Wilkinson, M., Haszeldine, R.S., Fallick, A.E., 2006. Hydrocarbon filling and leakage history of a deep geopressured sandstone, Fulmar Formation, United Kingdom North Sea. AAPG (Am. Assoc. Pet. Geol.) Bull. 90, 1945–1961.
Xu, Enai, Wang, Qingkui, 2016. Redefinition of Mesozoic stratigraphic and sedimentary characteristics in Kongnan area, Huanghua depression. Sino-Global Energy 21, 50–56 (In Chinese with English abstract).
Yuan, G., Cao, Y., Gluyas, J., Li, X., Xi, K., Wang, Y., Jia, Z., Sun, P., Oxtoby, N.H., 2015a. Feldspar dissolution, authigenic clays, and quartz cements in open and closed sandstone geochemical systems during diagenesis: typical examples from two sags in Bohai Bay Basin, East China. AAPG (Am. Assoc. Pet. Geol.) Bull. 99, 2121–2154.
Yuan, G., Gluyas, J., Cao, Yingchang, 2015b. Diagenesis and reservoir quality evolution of the eocene sandstones in the northern Dongying sag, Bohai Bay Basin, east China. Mar. Petrol. Geol. 62, 77–89.
Yuan, G., Cao, Y., Zhang, Y., Gluyas, J., 2017. Diagenesis and reservoir quality of sandstones with ancient “deep” incursion of meteoric freshwater——an example in the Nanpu Sag, Bohai Bay Basin, East China. Mar. Petrol. Geol. 82, 444–464.
Zan, N., Cao, Y., Wang, Y., et al., 2020. Geologic CO_2 storage in arkosic sandstones with $CaCl_2$-rich formation water. Chemical Geology 2020, 558.
Zhang, T., Zhang, M., Bai, B., Wang, X., Li, L., 2008. Origin and accumulation of carbon dioxide in the Huanghua depression, Bohai Bay Basin, China. AAPG (Am. Assoc. Pet. Geol.) Bull. 92, 341–358.
Zhang, F., Wu, Z., Li, 2019. Structural characteristics and its tectonic evolution of Huanghua depression during the Indosinian –Yanshan. J. China Inst. Min. Technol. 48, 842–857 (In Chinese with English abstract).
Zhao, X., Jin, F., Wang, Q., Bai, G., 2015. Buried-hill play, jizhong depression, Bohai Bay Basin: a review and future prospectivityBuried-hill play, jizhong subbasin, Bohai Bay Basin. AAPG (Am. Assoc. Pet. Geol.) Bull. 99, 1–26.
Zhao, X., Zhou, L., Pu, X., Jiang, W., 2018. Hydrocarbon-generating potential of the upper Paleozoic section of the Huanghua depression, Bohai Bay Basin, China. Energy Fuels 32, 12351–12364.
Zhao, X., Pu, X., Jiang, W., et al., 2019. An exploration breakthrough in Paleozoic petroleum system of Huanghua depression in Dagang Oilfield and its significance. Petrol. Explor. Dev. 46, 621–632 (In Chinese with English abstract).
Zhou, L., Wang, X., Fu, L., et al, 2019. Discovery and geological signifi cance of the Permian sandstone condensate gas reservoir in Wumaying buried hill, Huanghua depression. China Petrol. Explor. 24, 431-438 (In Chinese with English abstract).